JAAS

PAPER

View Article Online
View Journal | View Issue

Cite this: J. Anal. At. Spectrom., 2019, 34, 274

Binding effects in sulfur Kα and Kβ X-ray emission spectra

E. Sánchez,[a] M. Torres Deluigi[ab] and G. Castellano *[c]

Received 16th October 2018
Accepted 20th November 2018

DOI: 10.1039/c8ja00345a

rsc.li/jaas

A systematic study has been carried out in order to investigate the influence of the chemical bond on the occurrence of different sulfur decays to 1s vacancy states induced by electron impact. A number of samples in different oxidation states (+4, +6, 0 and −2) were irradiated in a commercial microscope, acquiring Kα and Kβ spectra for all sulfur oxidation states. Special attention has been paid to the case of emissions associated with decays corresponding to multiple ionizations. An important achievement of the present study is the high resolution obtained in the wavelength-dispersive spectra acquired with a commercial spectrometer.

1 Introduction

Sulfur is an essential component in biochemical systems like amino acids, vitamins, bacteria, proteins, and iron sulfur groups used in electron transfer and catalysis.[1,2] Environmental concerns range from natural and anthropogenic emissions of pollutive sulfur gases (H_2S, SO_2, and SO_3)[3] to the acidification of surface or underground waters by mining activities[4] or long range aerosol transport.[5]

A deep understanding of the sulfur chemical environment is required to obtain a detailed comprehension of the processes in which this element is involved.[6] Only a few techniques can provide direct information about the sulfur electronic structure, among which X-ray emission allows one to investigate the fine structure of photons emitted from atom relaxation to inner shell vacancies. The individual vacancy filling is well understood, particularly for pure samples, and gives rise to the so-called diagram lines. Satellite lines arise from multiple processes or in cases where binding atoms influence the characteristic emission, and they may provide information about the atomic inner electron correlation, the excitation dynamics, the relaxation process, and other effects influencing X-ray emission.[7–14]

A number of studies have been carried out to investigate satellite emission in different elements and compounds, excited by X-ray photons,[15–21] by protons,[22–25] by heavy ions[26–30] and by electrons,[7,8,31–35] and several theoretical approaches have been suggested.[36–44] Satellite lines appear in the spectral neighborhood of $K\alpha_1$ and $K\alpha_2$ diagram lines, namely, $K\alpha_{22}$ in the low-energy region,[9,45] $K\alpha''$[46] and $K\alpha'$,[47] with energies above the main Kα peaks, and also the emissions $K\alpha_3$ and $K\alpha_4$, corresponding to double vacancies,[48–54] and $K\alpha_5$ and $K\alpha_6$ corresponding to triple vacancies,[55,56] also with energies higher than the $K\alpha_1$ emission. It is worth mentioning that although the notation for decays associated with double and triple vacancy states is not uniform in the literature, in the present work it has been chosen to agree with that of the most recent studies, particularly using electron impact.[35,55] The satellite emissions $K\alpha'$, $K\alpha_3$ and $K\alpha_4$ arise from transitions occurring in the presence of 2p spectator holes,[31,47,49] whereas $K\alpha_5$ and $K\alpha_6$ involve triple ionizations accompanied by two 2p spectator holes.[29] The $K\alpha_{22}$ satellite line may be attributed to an energy level distortion due to the presence of 3d spectator holes.[20,36] Another explanation is based on KLM radiative Auger emission (RAE) processes, by which the initial K-shell vacancy is filled by a $2p_{1/2} \rightarrow 1s$ or $2p_{3/2} \rightarrow 1s$ decay, the energy balance being completed through the joint emission of an X-ray photon and an M-shell Auger electron.[9,57,58]

In the Kβ spectral region, the most intense diagram line $K\beta_{1,3}$ is surrounded by double ionization emissions like $K\beta^{III}$ and $K\beta^{IV}$,[8,59] and also Kβ′ and Kβ″ structures. In the case of sulfides, the $K\beta_{1,3}$ main peak has four components: $K\beta^{A}$, $K\beta^{B}$, $K\beta^{C}$ and $K\beta^{D}$.[60,61] $K\beta^{III}$ and $K\beta^{IV}$ lines originate from $1s \rightarrow 3p$ decays, also in the presence of 2p spectator holes.[8,22,24,26] Density functional theory calculations in sulfites and sulfates[45] reveal that the structure known as Kβ′ arises from transitions involving oxygen 2s orbitals; it has also been shown that the Kβ″ line, which distorts the high energy region of the $K\beta_{1,3}$ diagram line, mainly originates from transitions involving oxygen 2p orbitals.

Unfortunately, up to now no systematic study has been carried out for all sulfur oxidation states. In the present work, sulfur Kα and Kβ satellite lines have been carefully studied, after electron impact on different compounds, in order to investigate the influence of the chemical bond on the

[a]Departamento de Física, Universidad Nacional de San Luis, Argentina
[b]INQUISAL, CONICET, Argentina
[c]FaMAF, Universidad Nacional de Córdoba, Instituto de Física Enrique Gaviola (IFEG), CONICET, Argentina. E-mail: gcas@famaf.unc.edu.ar

occurrence of the different decays, particularly those corresponding to multiple ionizations. Special attention has been paid to the case of the emission energies corresponding to decays associated with triple vacancy states. One of the main challenges of the present work is to finely discriminate emission lines which usually cannot be deconvoluted in spectra acquired with commercial equipment like that used here, and therefore experimental mounts specifically designed for these kinds of measurements must be used.[25,44,61,62]

2 Experimental

Samples containing sulfur in different oxidation states (+4, +6, 0 and −2) were irradiated in a LEO 1450VP scanning electron microscope coupled with an INCA WAVE 700 wavelength dispersive spectrometer (WDS). The compounds studied were: sodium metabisulfite, $Na_2S_2O_5$ (+4); different sulfates, namely, $K_2S_2O_7$ potassium pyrosulfate, $K_2S_2O_8$ potassium persulfate, $CaSO_4$ anhydrite, $BaSO_4$ barium sulfate and Na_2SO_4 sodium sulfate (+6); sulfides (−2): ZnS zinc sulfide, FeS_2 iron sulfide, $(Fe,Ni)_9S_8$ pentlandite, HgS mercury sulfide, MoS_2 molybdenum disulfide, PbS lead sulfide and Sb_2S_3 antimony trisulfide; pure sulfur (0), and two compounds with mixed oxidations states: $Na_2S_2O_3$ sodium thiosulfate (−2; +6) and $K_2S_2O_5$ potassium metabisulfite or pyrosulfite (+4; +6). Some of these compounds—$CaSO_4$, ZnS, FeS_2, $(Fe,Ni)_9S_8$, HgS, MoS_2, PbS and Sb_2S_3—correspond to an SPI #02753-AB mineral standard set (serial number: 05-133); others are powder compounds, which were compacted under a constant pressure of 20 t cm^{-2}, and in order to ensure thermal and electrical conductivity, samples were coated with a 40 nm carbon layer.

X-ray photons of interest were induced by electron impact, and the resulting spectra were acquired through the WDS system, for which the take-off angle is 29°. Several analyzing crystals in Johansson geometry are available in this WDS, the most suitable for the spectra required in this work being a PET (pentaerythrite) crystal ($2d$ = 8.742 Å). Two proportional counters in tandem allow a high acquisition efficiency: a P10 (90% Ar to 10% CH_4) gas flow counter and a sealed Xe one. The electron incident energy chosen was 20 keV, whereas the probe current was set to around 80 nA, being monitored before and after spectrum acquisition in order to check stability. The narrowest 0.1 mm collimator aperture available was chosen with the aim of achieving the best energy resolution, which resulted in a 0.107 eV FWHM for the S-K$\beta^{A}_{1,3}$ line and a 0.093 eV FWHM for the S-Kα_1 diagram emission.

Two spectral ranges were rastered in each sample: from 2283.06 eV to 2365.84 eV with the aim of registering all Kα decays, and from 2440.35 eV to 2530.00 eV for the Kβ group. Spectra were acquired in order to ensure acceptable statistics in all peaks: the maximum intensity recorded was at least 1000 counts for Kβ emission and at least of 150 counts for Kα_3 or Kα_4 emissions. The background contribution was subtracted using a linear fit, which in the case of Kβ lines involved the step corresponding to the K-absorption edge. Spectra were analyzed as a function of wavelengths using the software PeakFit v4.12, which involves least-squares fitting, associating a Voigt function to each peak and Gaussian/Lorentzian area (AutoFit Peaks I Residuals). This Voigt function[63] is the convolution of a Gaussian distribution associated with the spectrometer response, and a Lorentzian function whose spreading is related to the mean lifetime of the ionized state.[64] In the analysis of Kβ and Kα spectra, peak fitting was carried out so that the Gaussian width assigned to all lines was the same, since the experimental apparatus influence is constant in the energy range scanned; the corresponding Lorentzian widths instead were allowed to vary, since they depend on the mean lifetime of the excited states intervening in the different transitions and therefore are characteristic of each decay. In the case of the Kα spectra, the fitting procedure for pure sulfur was completed first, achieving the same Lorentzian widths for Kα_1 and Kα_2, which were afterwards used as constants in the other spectra.

The recorded spectra were carefully calibrated, since slight temperature fluctuations may be reflected in important variations in the PET crystal response, because of its non-negligible linear expansion coefficient.[65] This calibration was accomplished by observing the shift in the pure Si Kα_1 line, where the crystal bears its optimal resolution; this shift was then assigned to the rest of the measured spectra.

X-ray absorption is another important correction taken into account in the assessment of each peak intensity area. The approach used for this aim is that proposed by Packwood and Brown[66] modified by Riveros *et al.*,[67] which implicitly involves the mentioned absorption effects. These intensities were also corrected accounting for the absolute efficiency of the spectrometer used, following ref. 68. With this approach, the spectrometer efficiencies of the equipment involved in the present measurements were determined by these authors for different crystals, particularly the PET analyzer used in this work. This absolute efficiency characterization is based on the comparison of spectra measured with each wavelength dispersive system and those acquired with an energy dispersive spectrometer. The inclusion of all the corrections mentioned means all experimental factors have been taken into account in the present work.

3 Results and discussion

3.1 Kα lines

Fig. 1 displays a spectrum recorded for a $CaSO_4$ sample, showing all the S-Kα lines that could be identified. Deconvoluted lines are also shown, according to the procedure depicted above. The intensity and energy shift occurring for each emission depend on different factors, which will be discussed separately for single and multiple primary vacancies. Roughly, single vacancies are associated with the most intense emission lines, whereas multiple ionizations are less likely, and the corresponding lines are therefore less intense—other excitation sources like protons show an opposite behavior.[26]

3.1.1 Kα$_1$, Kα$_2$ and Kα$_{22}$ lines. Although the Kα_1 emission originates from the $1s_{1/2} \rightarrow 2p_{3/2}$ decay, the energy associated with this line exhibits slight although appreciable shifts, depending on the oxidation state of the sulfur atoms involved in each compound, as shown in Fig. 2, where the Kα_{22}, Kα_1, Kα_2

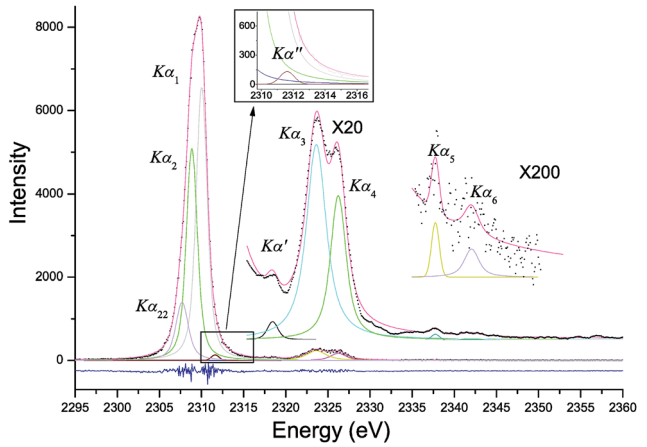

Fig. 1 Experimental $CaSO_4$ spectrum (dots) evidencing the principal and satellite lines in the sulfur Kα diagram emission region. The different continuous lines correspond to the fitting achieved.

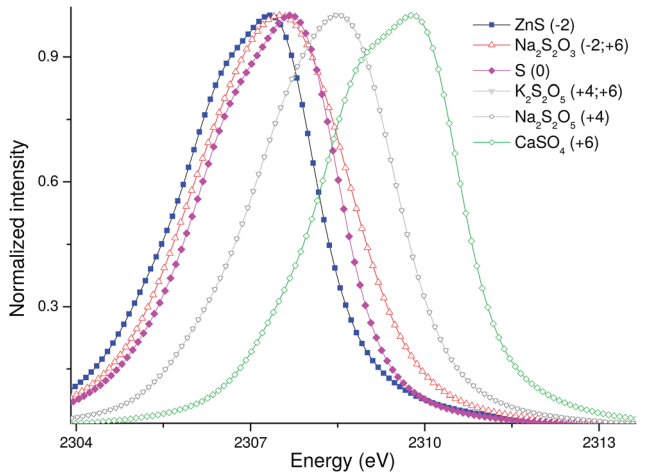

Fig. 2 Normalized X-ray spectra around the S-Kα_1 diagram region for different compounds involving various sulfur oxidation states: ZnS (−2); $Na_2S_2O_3$ (−2; +6); S (0); $K_2S_2O_5$ (+4; +6); $Na_2S_2O_5$ (+4) and $CaSO_4$ (+6).

and Kα″ contributions were appropriately deconvoluted in the main peaks for some of the compounds studied. It must be emphasized that the experimental strategy followed led to very accurate energy fits for the peak centroids, particularly in the most intense emissions; this is intimately related to the good energy resolution achieved, as well as the high statistics attained in the acquisition of the lines considered. The uncertainties reported by the software PeakFit quoted above correspond to 95% confidence interval, and the repeatability of these results was checked across the subsequent measurements performed in the present work.

Table 1 evidences that higher oxidation states correspond to higher Kα_1 emission energies, which has also been suggested by other authors.[8,62,69,70] A comparison with other data in the literature is displayed in Fig. 3. As the sulfur oxidation state bears higher values, the gap between the $1s_{1/2}$ and $2p_{3/2}$ increases, or since the core energy level $1s_{1/2}$ remains unchanged, the energy eigenvalue for the $2p_{3/2}$ is higher; these increases in the $2p_{3/2}$ level are consequences of the changes in the bonds occurring in the valence band. In the case of sulfides (−2), the sulfur atom hosts two additional electrons in the valence bands, which implies that the inner energy levels are decreased as compared with the neutral state.

In fact there is no clear evidence about a unique emission energy associated with each oxidation state, but slight differences appear depending on which element is bound to the sulfur atom. Bearing this in mind, energy ranges can be defined for the Kα_1 position for each oxidation state: sulfides between 2307.51 eV and 2307.82 eV, metabisulfites between 2308.83 eV and 2308.85 eV, and sulfates between 2308.94 eV and 2310.01 eV. Among the compounds studied, it is worth mentioning the particular behavior for $Na_2S_2O_3$ sodium thiosulfate (−2; +6) and $K_2S_2O_5$ potassium metabisulfite (+4; +6), which have two sulfur atoms with different oxidation states, as indicated between brackets. The sulfate character of these compounds is not evidenced in the spectra, since the Kα_1 line energy in the first case is within the sulfide range, whereas in the second the energy is similar to that of the sulfite range.

It can be readily seen from Table 1 that not only the Kα_1 energy is shifted because of the different bonds, but all the electron levels are modified, emission energies varying according to the corresponding oxidation state. The electron binding energies are modified as a whole in the level $n = 2$, relative changes in subshells being less important; this issue is evidenced in the fact that linewidths are quite well maintained when the oxidation state varies (see Fig. 2).

All these shifts in the emission energies (Kα_x − Kα_1) are displayed in Table 1. It can be seen that in the sulfite and the $Na_2S_2O_3$ compound, the Kα_2 emission energies are reduced from the S(0) state noticeably more than the shift corresponding to sulfides, sulfates and the $K_2S_2O_5$ compound. This means that when the sulfur oxidation state changes from 0 to a different state, the energy difference between the $2p_{3/2}$ and $2p_{1/2}$ levels always increases: slightly for oxidation states −2 and +6 and the $K_2S_2O_5$ compound, and more markedly for the state +4 and the $Na_2S_2O_3$ compound.

The Kα_{22} decay originates from KLM RAEs,[47,58,71–73] consisting in decays from the 2p shell, which means that the corresponding energy shifts have to be explained according to the different oxidation states, as done with the Kα_2 emission. This is clearly evidenced in the fact that the smallest energy shift from the Kα_1 line occurs for pure sulfur. Instead, these shifts slightly increase for the −2 and +6 oxidation states, and also for the $K_2S_2O_5$ compound, whereas the sulfite and the $Na_2S_2O_3$ compound bear larger differences. Although this behavior is quite similar to that observed for the Kα_2 emission, it must be noted that the energy shifts in the Kα_{22} emission for the sulfite and the $Na_2S_2O_3$ compound do not coincide; this means that the kinetic energies of the ejected Auger electrons involved in these transitions differ according to the sulfur oxidation state: the minimum energy of the Auger electrons is smaller for S(0), a bit higher in the case of sulfides, sulfates and the $K_2S_2O_5$ compound, and more important for the sulfite and the $Na_2S_2O_3$ compound.

Table 1 Fitted energies for the $K\alpha_1$, $K\alpha_2$ and $K\alpha_{22}$ peaks for the different sulfur compounds studied. Uncertainties in the last digits are shown in parentheses in the corresponding column headers

Oxidation state	Compound	Energy (eV)			RTP [% $K\alpha_1$]		Energy difference to $K\alpha_1$ (eV)	
		$K\alpha_{22}$ (1)	$K\alpha_2$ (1)	$K\alpha_1$ (1)	$K\alpha_{22}$	$K\alpha_2$	$K\alpha_{22}$ (2)	$K\alpha_2$ (2)
4	$Na_2S_2O_5$	2305.76	2307.49	2308.84	10.8(6)	75(1)	−3.08	−1.35
−2; 6	$Na_2S_2O_3$	2304.41	2306.47	2307.83	0.9(1)	47.9(8)	−3.42	−1.36
4; 6	$K_2S_2O_5$	2306.39	2307.62	2308.81	27(2)	79(1)	−2.42	−1.19
6	$K_2S_2O_7$	2306.83	2308.01	2309.16	36(2)	85(1)	−2.33	−1.15
6	$K_2S_2O_8$	2306.76	2307.95	2309.14	18(1)	72(1)	−2.38	−1.19
6	$CaSO_4$	2307.68	2308.84	2310.00	25(1)	78(1)	−2.32	−1.16
6	$BaSO_4$	2307.42	2308.77	2309.99	12.7(8)	78(1)	−2.57	−1.22
6	Na_2SO_4	2306.40	2307.74	2308.95	15.0(9)	73(1)	−2.55	−1.21
0	S	2305.86	2306.76	2307.89	30.3(7)	63.4(5)	−2.03	−1.13
−2	ZnS	2305.30	2306.35	2307.52	19(1)	66(1)	−2.22	−1.17
−2	FeS_2	2305.61	2306.63	2307.78	21(1)	59(1)	−2.17	−1.15
−2	$(Fe,Ni)_9S_8$	2305.28	2306.57	2307.81	8.6(5)	67(1)	−2.53	−1.24
−2	HgS	2305.27	2306.59	2307.81	14.5(9)	66(1)	−2.54	−1.22
−2	MoS_2	2305.48	2306.61	2307.81	29(2)	67(1)	−2.33	−1.20
−2	PbS	2305.41	2306.60	2307.78	14.8(9)	67(1)	−2.37	−1.18
−2	Sb_2S_3	2305.39	2306.45	2307.60	24(1)	67(1)	−2.21	−1.15

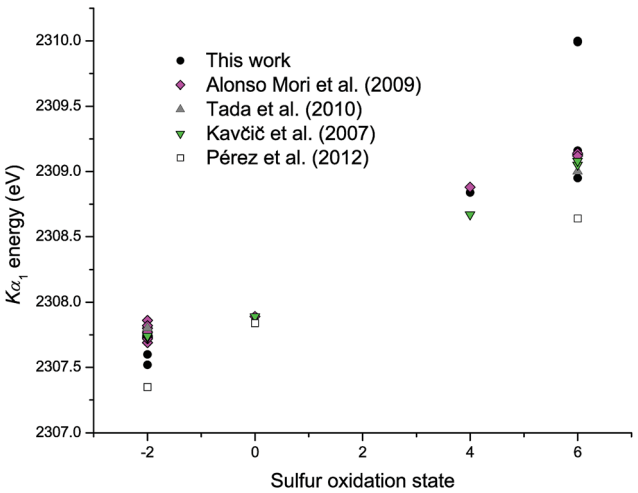

Fig. 3 Sulfur $K\alpha_1$ emission energies for the different oxidation states, as obtained in this work and by other authors.

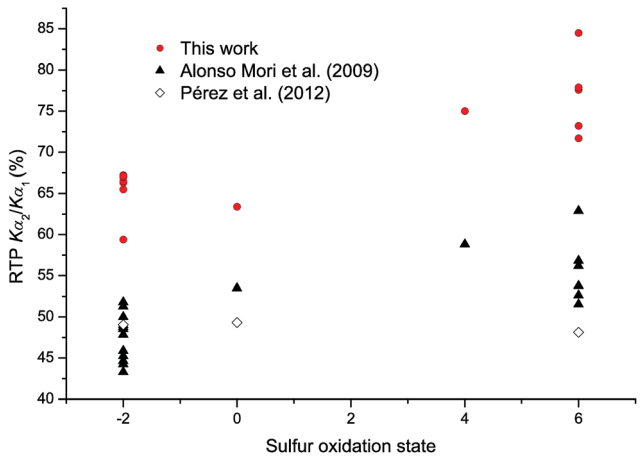

Fig. 4 Comparison of the sulfur $K\alpha_2/K\alpha_1$ RTPs obtained for the different oxidation states with values from the literature.

Another important issue to take into account is the possible variations in the radiative decay probabilities for the different sulfur oxidation states. To this aim, the relative transition probabilities (RTPs) were assessed as the ratio between the corresponding emission intensity $K\alpha_x$ and the $K\alpha_1$ line. Table 1 includes the RTPs for the $K\alpha_{22}$ and $K\alpha_2$ lines. It can be seen that no clear trend is evidenced for the $K\alpha_{22}$ line; only the $Na_2S_2O_3$ compound exhibits a distinctive behavior, bearing very low values for both lines. In the case of the $K\alpha_2$ line, the variations for the different oxidation states may be divided into two groups: pure sulfur and sulfides with RTPs between 59.4% and 67.2%, and sulfates, sulfites and the $K_2S_2O_5$ compound between 71.7% and 84.5%. In Fig. 4, the $K\alpha_2/K\alpha_1$ RTPs obtained here are compared with data from the literature. The values obtained by Alonso-Mori *et al.*[62] through synchrotron radiation are generally higher than the present results, though they follow a similar trend. This behavior suggests that the $2p_{1/2} \rightarrow 1s_{1/2}$ RTP depends on the sulfur oxidation state, being higher when sulfur is bound with valence +4 and +6. On the other hand, the data obtained by Pérez *et al.*[70] through electron impact are closer to the values obtained from ref. 62, however bearing a constant behavior for the different sulfur oxidation states.

3.1.2 Kα″, Kα′, Kα$_3$, Kα$_4$, Kα$_5$ and Kα$_6$ lines. Satellite lines corresponding to double vacancies are called Kα″, Kα′, Kα$_3$ and Kα$_4$,[17,36,48,50,52,53,74] whereas triple vacancy lines are known as Kα$_5$ and Kα$_6$.[36,55] Some of them are displayed in Fig. 5 for different sulfur compounds. In the case of the lowest energy line Kα″, the spectator hole is present in the sulfur *M* shell ($n = 3$), and the electron transition 2p → 1s occurs from the L to K shell.[7,46,47] Only a few examples have been published demonstrating this emission for sulfur,[7,46] which will be extended here for all the

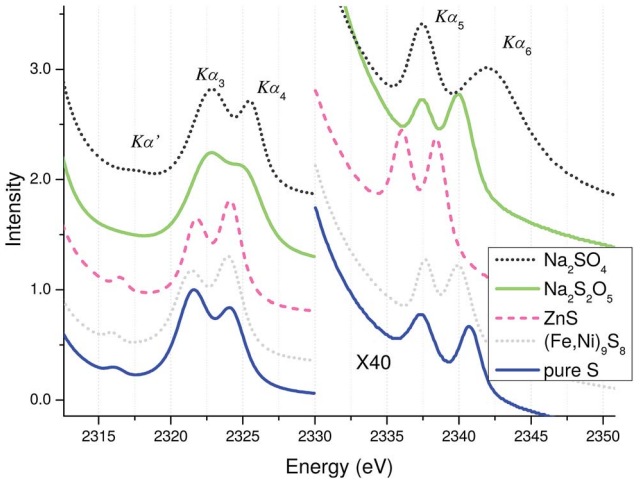

Fig. 5 Satellite lines Kα′, Kα$_3$, Kα$_4$, Kα$_5$ and Kα$_6$ around the main sulfur Kα$_1$ line for pure sulfur and the compounds $(Fe,Ni)_9S_8$, ZnS, $Na_2S_2O_5$ (4) and Na_2SO_4 (6). Intensities have been normalized to the peak maxima, and the ordinates have been shifted in the different plots for easy visualization.

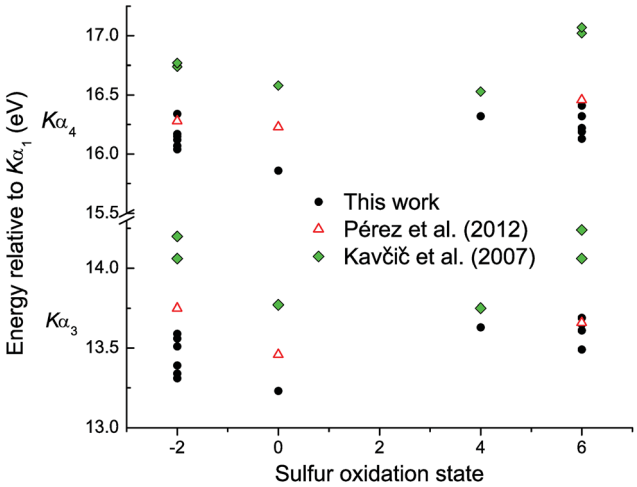

Fig. 6 Kα$_3$ and Kα$_4$ emission energies relative to the Kα$_1$ line for the different oxidation states.

compounds studied. From Table 2 it can be seen that most compounds bear a Kα″ emission energy which differs from the Kα$_1$ energy between 1.2 eV and 1.7 eV, with the exceptions of sodium metabisulfite, 2.8 eV above the Kα$_1$ emission, and sodium thiosulfate, for which the Kα″ is only 0.7 eV above Kα$_1$. The spectator hole in the M shell therefore modifies in a similar way the electron eigenenergies corresponding to the 2p levels in the different oxidation states.

The lines labeled Kα′, Kα$_3$ and Kα$_4$ (see Fig. 5) correspond to double vacancy emissions, with a spectator hole in the L shell. The Kα′ line originates from the transition $[1s2p]^1P \rightarrow [2p^2]^1S$,[75] and the fitted energies are between 7.6 eV and 8.7 eV. On the other hand, the Kα$_3$ and Kα$_4$ emissions respectively correspond to the transitions $[1s2p]^3P \rightarrow [2p^2]^3P$ and $[1s2p]^1P \rightarrow [2p^2]^1D$.[7,71]

As shown in Table 2 and Fig. 6, the emission energies in sulfides are slightly higher than those in sulfites, and lower than those in sulfates, a behavior already observed by other authors.[25,62]

As can be seen in Table 3, the Kα$_3$/Kα$_4$ intensity ratio is mostly above 1, with the exception of the sulfides $(Fe,Ni)_9S_8$ and PbS. This ratio Kα$_3$/Kα$_4$ appears to separate sulfides and $Na_2S_2O_3$, with values between 0.88 and 1.3, sulfates, pure sulfur and $K_2S_2O_5$ between 1.53 and 2.33, and the sulfite with 2.82. As displayed in Fig. 7, these results roughly coincide with data from the literature.[7,25,52,62] Sulfates, however, bear quite a different behavior as compared to the data in ref. 25, which are greater than those obtained here. Such differences are to be expected, since those values were determined through proton irradiation, and the probability distribution of multiple vacancies depends on the projectile. Other minor discrepancies can be observed, but the wide number of compounds used here

Table 2 Fitted energies for the Kα″, Kα′, Kα$_3$, Kα$_4$, Kα$_5$ and Kα$_6$ peaks for the different sulfur compounds studied. Uncertainties in the last digits are shown in parentheses in the corresponding column headers

Oxidation state	Compound	Energy (eV)					
		Kα″ (2)	Kα′ (5)	Kα$_3$ (7)	Kα$_4$ (7)	Kα$_5$ (2)	Kα$_6$ (2)
4	$Na_2S_2O_5$	2311.6	2316.4	2322.47	2325.16	2337	2340
−2; 6	$Na_2S_2O_3$	2308.6	2316.5	2321.45	2324.08	2338	2341
4; 6	$K_2S_2O_5$	2310.3	2317.0	2322.42	2325.04	2338	2342
6	$K_2S_2O_7$	2310.8	2317.3	2322.65	2325.29	2338	2342
6	$K_2S_2O_8$	2310.6	2317.2	2322.79	2325.46	2337	2342
6	$CaSO_4$	2311.6	2318.4	2323.61	2326.22	2338	2342
6	$BaSO_4$	2311.5	2318.4	2323.48	2326.18	2338	2340
6	Na_2SO_4	2310.6	2317.5	2322.64	2325.36	2337	2342
0	S	2309.3	2315.8	2321.12	2323.75	2336	2340
−2	ZnS	2309.0	2315.8	2321.08	2323.69	2336	2340
−2	FeS_2	2309.3	2315.7	2321.17	2323.90	2338	2340
−2	$(Fe,Ni)_9S_8$	2309.3	2316.2	2321.37	2324.15	2338	2340
−2	HgS	2309.3	2315.8	2321.15	2323.88	2335	2339
−2	MoS_2	2309.2	2316.0	2321.32	2323.93	2337	2341
−2	PbS	2309.0	2316.1	2321.37	2323.93	—	—
−2	Sb_2S_3	2309.1	2315.6	2320.91	2323.64	2337	2341

Table 3 Transition probabilities for the Kα″, Kα′, $Kα_3$ and $Kα_4$ peaks relative to $Kα_1$ emission for the different sulfur compounds studied

Oxidation state	Compound	RTP (% $Kα_1$) Kα″	Kα′	$Kα_3$	$Kα_4$	$Kα_3/Kα_4$ RTP ratio
4	$Na_2S_2O_5$	0.6(5)	0.33(7)	8(1)	3.0(4)	2.8(7)
−2; 6	$Na_2S_2O_3$	0.8(7)	0.15(3)	4(6)	3.5(5)	1.2(3)
4; 6	$K_2S_2O_5$	0.8(7)	0.05(1)	8(1)	3.8(5)	2.1(5)
6	$K_2S_2O_7$	1.0(9)	0.16(3)	7(1)	5.1(7)	1.4(3)
6	$K_2S_2O_8$	1.6(9)	0.14(3)	8(1)	3.5(5)	2.3(6)
6	$CaSO_4$	1.1(9)	0.31(6)	7(1)	3.9(6)	1.8(4)
6	$BaSO_4$	0.7(6)	0.32(6)	6.5(9)	4.3(6)	1.5(4)
6	Na_2SO_4	0.7(6)	0.26(5)	7(1)	3.2(5)	2.4(6)
0	S	0.9(3)	0.11(2)	6.5(4)	4.0(3)	1.6(2)
−2	ZnS	0.8(7)	0.18(4)	4.9(7)	4.7(7)	1.0(2)
−2	FeS_2	0.5(4)	0.11(2)	5.2(7)	4.3(6)	1.2(3)
−2	$(Fe,Ni)_9S_8$	0.7(6)	0.36(7)	3.9(5)	4.4(6)	0.9(2)
−2	HgS	1.6(9)	0.6(1)	5.4(8)	4.2(6)	1.3(3)
−2	MoS_2	4(1)	0.3(6)	5.5(8)	5.2(7)	1.1(3)
−2	PbS	0.5(4)	0.3(6)	4.6(6)	4.9(7)	0.9(2)
−2	Sb_2S_3	1.4(9)	0.2(3)	5.2(7)	5.0(7)	1.0(2)

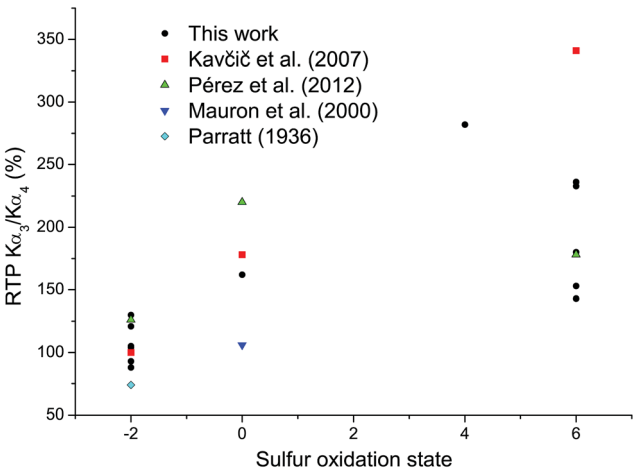

Fig. 7 Relative transition probabilities $Kα_3/Kα_4$ for the different oxidation states.

allows us to avoid isolated behaviors. Summarizing, the RTP ratios for these lines in sulfates behave like pure sulfur, whereas the $Na_2S_2O_3$ ratio follows the trend of −2 oxidation state compounds instead of +6, and $K_2S_2O_5$ accommodates its RTPs like +6 bonds instead of +4.

Although the triple vacancy lines in this group ($Kα_5$ and $Kα_6$) are rather weak, their emission energies were successfully identified, as displayed in Table 2. No definite trend can be observed in these cases for the different oxidation states.

3.2 Kβ lines

3.2.1 Single vacancy emissions: $Kβ_{1,3}$, $Kβ^A$, $Kβ^B$, $Kβ^C$, $Kβ^D$, Kβ′, Kβ″, $Kβ_x$ and $Kβ_{xx}$. $Kβ_{1,3}$ is the most intense emission of this group, and originates mainly from 3p → 1s transitions. Fig. 8 displays the intensity interval measured in the different oxidation states, energy shifts being minimum for sulfates (+6),

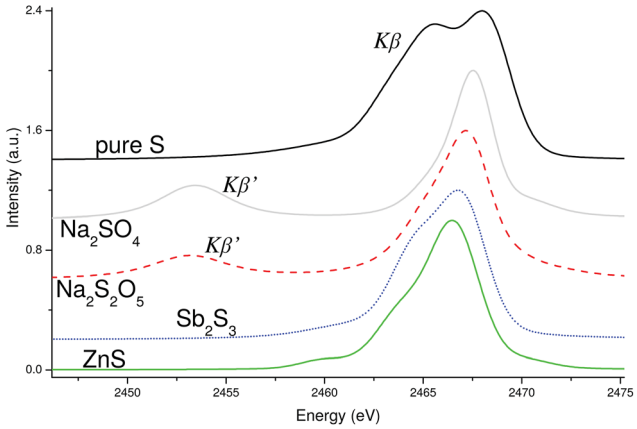

Fig. 8 Kβ and Kβ′ emissions for the different compounds studied. Intensities have been normalized to the peak maxima, and the ordinates have been shifted in the different plots for easy visualization.

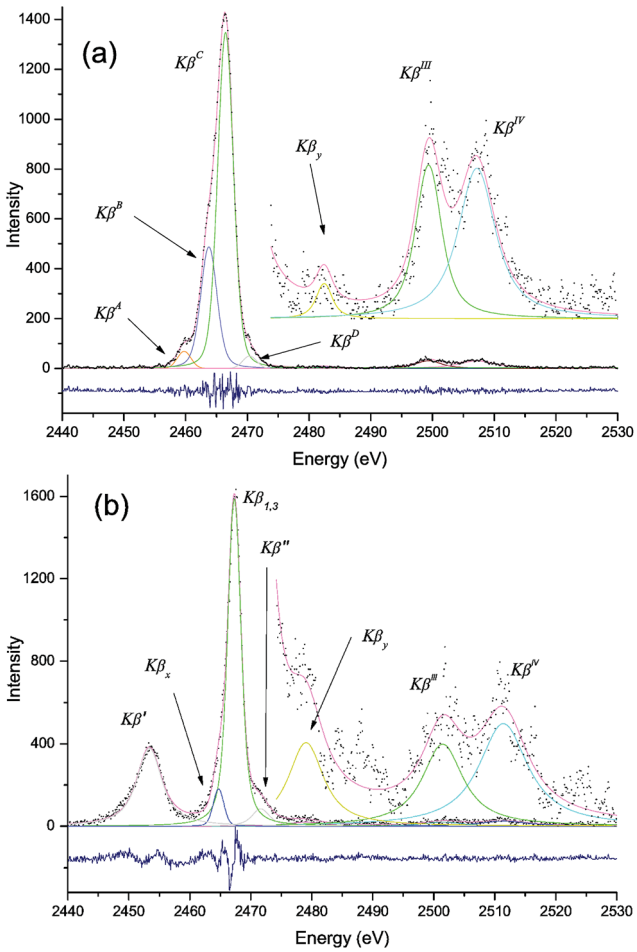

Fig. 9 Experimental (dots) Kβ emissions for ZnS (a) and $CaSO_4$ (b). In both cases the $Kβ_y$, $Kβ^{III}$ and $Kβ^{IV}$ lines are present, whereas only ZnS bears $Kβ^A$, $Kβ^B$, $Kβ^C$ and $Kβ^D$ (a), and only $CaSO_4$ bears $Kβ_{1,3}$, $Kβ_x$, Kβ′ and Kβ″ (b). The different continuous lines correspond to the fitting achieved.

intermediate for sulfites (+4), and maximum for sulfides (−2). This energy shift behavior as a function of the oxidation state was also observed by other authors.[18,21,61,62,76] By deconvoluting

Table 4 Fitted energies for the Kβ peaks corresponding to pure sulfur and the different compounds studied. Uncertainties in the last digits are shown in parentheses in the corresponding column headers

		Energy (eV)							
Oxidation state	Compound	Kβ′ (4)	Kβ$_x$ (3)	Kβ$_{1,3}$ (6)	Kβ″ (7)	Kβ$_{xx}$ (1)	Kβ$_y$ (2)	Kβ^{III} (5)	Kβ^{IV} (6)
4	$Na_2S_2O_5$	2452.80	2463.8	2466.65	2467.3	2471.4	2488	2500.6	2508.9
−2; 6	$Na_2S_2O_3$	2452.63	2463.9	2466.28	2472.1			2500.2	2508.5
4; 6	$K_2S_2O_5$	2452.67	2464.4	2466.79	2467.4	2471.2	2478	2500.8	2509.8
6	$K_2S_2O_7$	2452.91	2464.5	2467.21	2471.9		2478	2501.5	2511.4
6	$K_2S_2O_8$	2452.82	2463.6	2467.31	2472.5		2478	2501.2	2511.3
6	$CaSO_4$	2453.42	2464.8	2467.36	2471.7		2479	2501.5	2511.5
6	$BaSO_4$	2453.23	2464.3	2467.31	2471.8		2479	2501.3	2511.2
6	Na_2SO_4	2452.69	2464.6	2466.76	2470.8		2478	2501.7	2510.7

		Energy (eV)						
Oxidation state	Compound	Kβ$^D_{1,3}$ (3)	Kβ$^C_{1,3}$ (5)	Kβ$^B_{1,3}$ (3)	Kβ$^A_{1,3}$ (1)	Kβ$_y$ (2)	Kβ^{III} (2)	Kβ^{IV} (5)
0	S	2459.61	2463.65	2465.63	2468.23		2499.3	2506.2

		Energy (eV)						
Oxidation state	Compound	Kβ$_A$ (2)	Kβ$_B$ (6)	Kβ$_C$ (2)	Kβ$_D$ (2)	Kβ$_y$ (2)	Kβ^{III} (3)	Kβ^{IV} (4)
−2	ZnS	2459.2	2463.26	2465.97	2469.8	2481	2498.8	2506.6
−2	FeS_2		2463.38	2466.25	2469.4		2498.8	2506.2
	$(Fe,Ni)_9S_8$		2463.38	2465.17	2468.1		2498.1	2505.9
−2	HgS	2460.6	2464.19	2466.73	2470.8			—
−2	MoS_2		2463.34	2464.75	2467.0		2499.3	2507.7
−2	PbS	2461.7		2465.66	2467.4		2492.3	2501.8
−2	Sb_2S_3	2461.4	2464.70	2467.07	2469.8		2499.4	2506.9

these spectra, the intervening lines were readily identified in each acquired spectrum, as exemplified in Fig. 9. As emphasized above, the experimental strategy followed in this work led to very accurate energy fits for the centroids of the most intense peaks, which was also observed in the group of Kβ emissions. The main features about these lines are detailed in Tables 4 and 5. It is worth noting that the Kβ main peak in sulfides splits into 4 different lines (Fig. 9(a)), named Kβ^A, Kβ^B, Kβ^C and Kβ^D, with increasing energy.[61] Pure sulfur also exhibits 4 components in the main Kβ peak, namely Kβ$^A_{1,3}$, Kβ$^B_{1,3}$, Kβ$^C_{1,3}$ and Kβ$^D_{1,3}$ (decreasing energy); the first three were reported in ref. 60, whereas the last one has been added in the present work, since it was necessary to achieve an appropriate fit. These peak splittings were explained through theoretical assessments based on variational computations[41] and also by means of density functional theory[61] for the ZnS compound.

The main emission energies obtained here for the various oxidation states studied are shown in Fig. 10, as compared with the results from other authors.[21,60–62] It can be seen that sulfide emissions spread in a wide energy range, embracing the sulfite and sulfate ranges; this behavior is different for each sulfur compound, strongly depending on the ligand atom and also on the bond structure. Sulfite values are below those corresponding to sulfates, whose spreading is less pronounced, whereas the maximum values correspond to pure sulfur emission. This last issue differs from the behavior observed for the Kα$_1$ line (Fig. 3), since the 2p binding energies clearly decrease with the oxidation state; the 3p shell instead is less bound in the pure sulfur state than in compounds, although sulfur 3p electrons constitute the valence band and are *a priori* expected to evidence some trend with the oxidation state.

The S-Kβ relative intensities for the various components also vary in the different compounds, as can be seen from Table 5. The most intense Kβ′ emission, originating from molecular orbitals and only occurring in sulfates and sulfites, is stronger in sulfates, as supported in ref. 21 through X-ray excitation experiments. Another remarkable feature is that in sulfides, transition rates strongly depend on the atom bounded to sulfur. In ZnS, HgS and FeS_2, Kβ^D and the more intense Kβ^B peaks bear similar RTPs, which implies that the S – 3p level electron densities are also similar, since these emissions mainly depend on this central sulfur atom population, according to the assessments carried out in ref. 61 for ZnS.

3.2.2 Multiple vacancy emissions: Kβ^{III}, Kβ^{IV} and Kβ$_y$ lines. Double vacancy Kβ emissions have also been studied in this work. The lines named Kβ^{III} and Kβ^{IV} respectively originate from the transitions $[1s^{-1}2p^{-1}]^3P_2 \rightarrow [2p^{-1}3p^{-1}]^3D_3$ and $[1s^{-1}2p^{-1}]^1P_1 \rightarrow [2p^{-1}3p^{-1}]^1D_2$.[59] Although these emissions have been previously studied only in a few sulfur compounds,[70] in this work they have been analyzed for a variety of sulfur oxidation states. Fig. 11 shows the lines for S(0), $Na_2S_2O_5$, Na_2SO_4, Sb_2S_3 and ZnS, evidencing the differences in the emission energies as well as in their relative intensities. These normalized probabilities are similar for the different

Table 5 Relative transition probabilities for the Kβ lines, normalized to the main line of each group, for double vacancy transition emissions $K\beta^{III}$/$K\beta^{IV}$ for pure sulfur and the compounds studied

		RTP (% $K\beta_{1,3}$)							
Oxidation state	Compound	Kβ′	$K\beta_x$	Kβ″	$K\beta_{xx}$	$K\beta_y$	$K\beta^{III}$	$K\beta^{IV}$	$K\beta^{III}/K\beta^{IV}$
4	$Na_2S_2O_5$	26.3(1)	11.9(7)	0.4(1)	3.2(9)	0.2(2)	4.1(4)	4.7(5)	0.9(2)
−2; 6	$Na_2S_2O_3$	11.7(6)	12.7(8)	1.4(4)			5.1(6)	7.2(8)	0.7(1)
4; 6	$K_2S_2O_5$	41(2)	9.4(6)	1.4(4)	2.0(6)	4(1)	5.9(7)	8.6(9)	0.7(1)
6	$K_2S_2O_7$	39(2)	21(1)	0.9(3)		0.5(4)	5.9(6)	7.0(8)	0.8(2)
6	$K_2S_2O_8$	42(2)	15.0(9)	0.7(2)		1.4(6)	6.0(7)	6.1(7)	1.0(2)
6	$CaSO_4$	54(3)	8.0(5)	8(1)		5(2)	5.5(6)	8.2(9)	0.7(1)
6	$BaSO_4$	49(2)	12.9(8)	5.2(8)		2.1(9)	8.6(9)	6.5(7)	1.3(3)
6	Na_2SO_4	39(2)	7.4(4)	1.3(4)		1.9(9)	2.9(3)	6.3(7)	0.45(9)

		RTP (% $K\beta^{A}_{1,3}$)						
Oxidation state	Compound	$K\beta^{D}_{1,3}$	$K\beta^{C}_{1,3}$	$K\beta^{B}_{1,3}$	$K\beta_y$	$K\beta^{III}$	$K\beta^{IV}$	$K\beta^{III}/K\beta^{IV}$
0	S	29(3)	71(4)	69(2)		9.4(9)	13(1)	0.7(1)

		RTP (% $K\beta_C$)						
Oxidation state	Compound	$K\beta_A$	$K\beta_B$	$K\beta_D$	$K\beta_y$	$K\beta^{III}$	$K\beta^{IV}$	$K\beta^{III}/K\beta^{IV}$
−2	ZnS	4.4(3)	41.5(7)	4.0(3)	0.4(3)	5.5(6)	9.1(9)	0.61(7)
−2	FeS_2		49.3(8)	3.4(3)		5.0(5)	8.4(9)	0.59(7)
−2	$(Fe,Ni)_9S_8$		91(1)	18(1)		7.5(4)	10.7(7)	0.70(8)
−2	HgS	17.9(3)	43.3(7)	7.1(6)				
−2	MoS_2		20.2(3)	55(3)		7.5(6)	11.5(7)	0.65(8)
−2	PbS	7.4(6)		65(3)		24(2)	31(2)	0.79(9)
−2	Sb_2S_3	12.3(9)	92(1)	5.4(4)		7.3(6)	19(1)	0.38(6)

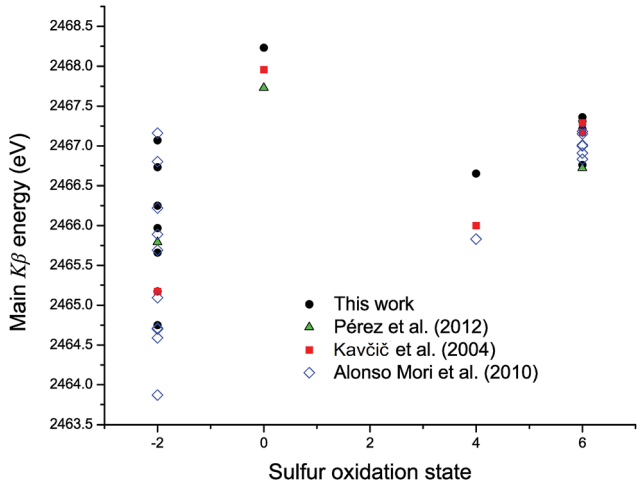

Fig. 10 Sulfur $K\beta_{1,3}$ emission energies for the different oxidation states.

compounds, with some exceptions in the case of sulfurs, with higher values; the maximum values corresponding to Sb_2S_3 for the $K\beta^{IV}$ line and PbS for both lines.

The $K\beta^{III}/K\beta^{IV}$ RTP ratios exhibit no definite variations for the different oxidation states. Most compounds bear values for this ratio between 0.59 and 0.87, with the exceptions of Sb_2S_3 (0.38) and Na_2SO_4 (0.45), with lower values, and $K_2S_2O_8$ (0.98) and $BaSO_4$ (1.32), with higher ratios. These probabilities therefore appear not to vary if the spectator hole locates in the L_2 or the L_3 subshell. The particular differences observed in some compounds are not associated with the oxidation state—as in the S-Kα double-vacancy spectrum—but might be attributed to other specific issues related to the chemical environment.

As can be seen in Table 4, the energy differences $K\beta^{IV} - K\beta^{III}$ slightly depend on the oxidation state, bearing the minimum value for pure sulfur, increasing for sulfides (with the exception of MoS_2 and PbS) and even more for metabisulfite, reaching the maximum values for sulfates. Compounds with mixed oxidation states ($Na_2S_2O_3$ and $K_2S_2O_5$) exhibit energy differences similar to those for sulfates.

The $K\beta_y$ line, also present in Fig. 11, has been reported only for sulfates in ref. 61. By analyzing the measurements performed in this work, this line evidently is present not only in sulfates, but is also observed in the sulfite Na_2SO_5 and in the sulfide ZnS, though with lower intensities. This suggests that its origin is related to the S(+6) and S(+4) electronic configurations, whereas in S(−2) it strongly depends on the sulfur chemical environment. For this reason careful characterization of this line was carried out, obtaining for sulfates and $K_2S_2O_5$ an energy shift between 10.4 and 11.7 eV, with RTPs ranging from 0.43% and 4.94%; for $Na_2S_2O_5$ the energy shift was 21.7 eV and the RTP, 0.24%, and finally the energy shift for ZnS was 14.9 eV with an RTP of 0.37%. These results evidence the strong influence of the oxidation states on the emission of this line.

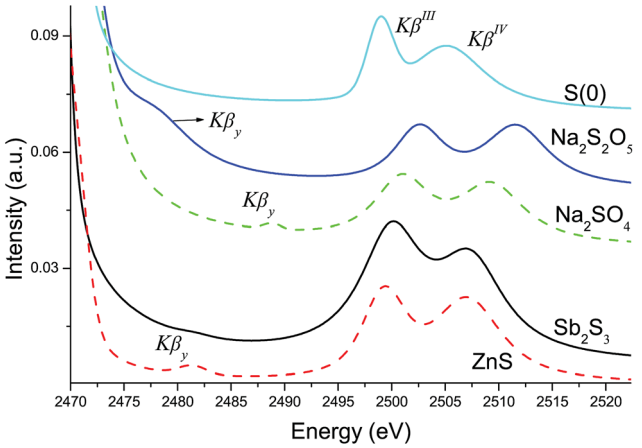

Fig. 11 Double vacancy satellite lines $K\beta^{III}$ and $K\beta^{IV}$ for pure sulfur and the compounds $Na_2S_2O_5$, Na_2SO_4, Sb_2S_3 and ZnS.

4 Conclusions

In the present work, it was possible to determine that the energy difference between $2p_{3/2}$ and 1s levels increases for increasing sulfur oxidation state (−2, 0, +4, and +6), as reflected in the analysis of the $K\alpha_1$ emissions. These changes in the $2p_{3/2}$ levels arise as a consequence of the chemical bonds involving the sulfur valence band. As a general behavior, all Kα emission shifts are similar to that of the main $2p_{3/2} \rightarrow 1s$ decay ($K\alpha_1$) shift, which means that the energies of the sulfur L-shell electrons are more affected in the chemical bonds, as expected. The $K\alpha_2$ emissions ($2p_{1/2} \rightarrow 1s$) suggest that the energy difference between the orbitals involved in compounds is always higher in pure sulfur; in particular, the $K\alpha_{22}$ emission energy increase in compounds implies that Auger electrons require higher incident energies than those in pure sulfur atoms. In addition, all emission energies associated with triple-vacancy states ($K\alpha_5$ and $K\alpha_6$ lines) were appropriately identified in all the compounds studied.

No clear trend in the main Kβ energy shifts was found, as in the case of $K\alpha_1$ emissions. It is worth mentioning that the Kβ main peak deconvolution performed in sulfides produced a splitting into 4 different lines ($K\beta^A$, $K\beta^B$, $K\beta^C$ and $K\beta^D$), as already found in ref. 61. Similarly, pure sulfur also exhibits four components in the main Kβ peak, as reported in ref. 44, which may be explained through variational computations.[41] The $K\beta_y$ line has been previously reported only in sulfates,[61] for which it is quite strong; in the present assessment it was also possible to clearly measure it in metabisulfites and in ZnS, despite its less intense emission. Further investigation about this emission may allow us to clarify if it indeed originates from a double-vacancy state accompanied by a spectator hole in the 3p orbital.

Although all the emission energies have been previously reported in several studies performed with different excitation sources, which have been complemented with theoretical calculations for the case of Na_2SO_3, Na_2SO_4 and ZnS,[61] the present analysis has been performed for the first time by electron impact, by using commercial equipment, and covering a wide variety of sulfur oxidation states.

A major achievement of the present work is the high resolution obtained in the spectra acquired with commercial equipment. Most FWHM values are slightly below 3 eV, which are often comparable with the resolution corresponding to wavelength dispersive experimental mounts specifically designed for these kinds of measurements.

Conflicts of interest

There are no conflicts to declare.

Acknowledgements

The authors gratefully acknowledge the Laboratorio de Microscopía Electrónica y Microanálisis of the Universidad Nacional de San Luis, Argentina, where measurements were carried out.

References

1 H. Beinert, R. H. Holm and E. Münck, *Science*, 1997, **227**, 653–659.
2 I. J. Pickering, G. N. George, E. Y. Yu, D. C. Brune, C. Tuschak, J. Overmann, J. T. Beatty and R. C. Prince, *Biochemistry*, 2001, **40**, 8138–8145.
3 B. Scaillet, *Science*, 2008, **319**, 1628–1629.
4 V. P. Evangelou and Y. L. Zhang, *Crit. Rev. Environ. Sci. Technol.*, 1995, **25**, 141–199.
5 S. Imai, Y. Yamamoto, T. Yamamoto, K. Kodama, J. Nishimoto and Y. Kikuchi, *Anal. Sci.*, 2018, **34**, 589–598.
6 V. Chubarov, A. Amosova and A. Finkelshtein, *X-Ray Spectrom.*, 2016, **45**, 352–356.
7 L. Parratt, *Phys. Rev.*, 1936, **50**, 1–15.
8 O. Keski-Rahkonen, E. Mikkola, K. Reinikainen and M. Lehkonen, *J. Phys. C: Solid State Phys.*, 1985, **18**, 2961–2975.
9 N. Maskil and M. Deutsch, *Phys. Rev. A*, 1988, **38**, 3467–3472.
10 S. N. Soni, *Phys. Lett. A*, 1997, **237**, 48–52.
11 M. Fritsch, C. C. Kao, K. Hämäläinen, O. Gang, E. Förster and M. Deutsch, *Phys. Rev. A*, 1998, **57**, 1686–1697.
12 J. Niskanen, C. J. Sahle, K. O. Ruotsalainen, H. Müller, M. Kavčič, M. Žitnik, K. Bučar, M. Petric, M. Hakala and S. Huotari, *Sci. Rep.*, 2016, **6**, 21012.
13 S. Fazinić, L. Mandić, M. Kavčič and I. Božičević, *J. Anal. At. Spectrom.*, 2011, **26**, 2467–2476.
14 J. R. Vegelius, K. O. Kvashnina, M. Klintenberg, I. L. Soroka and S. M. Butorin, *J. Anal. At. Spectrom.*, 2012, **27**, 1882–1888.
15 P. Chevallier, M. Tavernier and J. Briand, *J. Phys. B: At. Mol. Phys.*, 1978, **11**, L171.
16 G. R. Babu, V. Gopalakrishna, M. N. L. Raju, K. Parthasaradhi, V. R. K. Murty, M. V. R. Murti and K. S. Rao, *Phys. Rev. A*, 1987, **36**, 386–389.
17 K. Kawatsura, T. Morikawa, K. Takahiro, M. Oura, H. Yamaoka, K. Maeda, S. Hayakawa, S. Ito, M. Terasawa and T. Mukoyama, *J. Phys. B: At., Mol. Opt. Phys.*, 2003, **36**, 4065–4072.
18 M. Torres Deluigi, E. Perino, R. Olsina and A. Riveros de la Vega, *Spectrochim. Acta, Part B*, 2003, **58**, 1699–1707.

19 N. Shigeoka, H. Oohashi, T. Tochio, Y. Ito, T. Mukoyama, A. M. Vlaicu and S. Fukushima, *Phys. Rev. A*, 2004, **69**, 052505.
20 Y. Ito, T. Tochio, H. Oohashi and A. M. Vlaicu, *Radiat. Phys. Chem.*, 2006, **75**, 1534–1537.
21 M. Torres Deluigi and J. A. Riveros, *Chem. Phys.*, 2006, **325**, 472–476.
22 M. K. Kavčič, M. Budnar, A. Mühleisen and I. Török, *Nucl. Instrum. Methods Phys. Res., Sect. B*, 1998, **136**, 173–178.
23 M. Kavčič, *Phys. Rev. A*, 2003, **68**, 022713.
24 M. Uršič, M. Kavčič and M. Budnar, *Nucl. Instrum. Methods Phys. Res., Sect. B*, 2003, **211**, 7–14.
25 M. Kavčič, A. G. Karydas and Ch. Zarkadas, *Nucl. Instrum. Methods Phys. Res., Sect. B*, 2004, **222**, 601–608.
26 B. Hodge, R. Kauffman, C. F. Moore and P. Richard, *J. Phys. B: At. Mol. Phys.*, 1973, **6**, 2468–2472.
27 K. Jamison, C. Woods, R. Kauffman and P. Richard, *Phys. Rev. A*, 1975, **11**, 505–508.
28 K. Jamison, J. Hall, J. Oltjen, C. Woods, R. Kauffman, T. Gray and P. Richard, *Phys. Rev. A*, 1976, **14**, 937–945.
29 I. Török, T. Papp and S. Raman, *Nucl. Instrum. Methods Phys. Res., Sect. B*, 1999, **150**, 8–13.
30 I. Božičević Mihalić, S. Fazinić, T. Tadić, D. Cosic and M. Jakšić, *J. Anal. At. Spectrom.*, 2016, **31**, 2293–2304.
31 D. Fischer and W. Baun, *J. Appl. Phys.*, 1965, **36**, 534–537.
32 U. Misra and L. Watson, *Phys. Scr.*, 1987, **36**, 673–675.
33 G. Hölzer, M. Fritsch, M. Deutsch, J. Härtwig and E. Förster, *Phys. Rev. A*, 1997, **56**, 4554–4568.
34 D. Küchler, U. Lehnert and G. Zschornack, *X-Ray Spectrom.*, 1998, **27**, 177–182.
35 S. Limandri, A. Carreras, R. Bonetto and J. Trincavelli, *Phys. Rev. A*, 2010, **81**, 012504.
36 M. Deutsch, E. Förster, G. Hölzer, J. Härtwig, K. Hämäläinen, C.-C. Kao, S. Huotari and R. Diamant, *J. Res. Natl. Inst. Stand. Technol.*, 2004, **109**, 75–98.
37 F. A. Gianturco, *J. Phys. B: At. Mol. Phys.*, 1968, **1**, 614–619.
38 S. Salem, G. Hockney and P. Lee, *Phys. Rev. A*, 1976, **13**, 330–334.
39 M. Deutsch, *Phys. Rev. A*, 1989, **39**, 1077–1081.
40 M. Deutsch, *Phys. Rev. A*, 1989, **39**, 3956–3959.
41 E. Uda, J. Kawai and M. Uda, *Nucl. Instrum. Methods Phys. Res., Sect. B*, 1993, **75**, 24–27.
42 J. Kawai, *J. Electron Spectrosc. Relat. Phenom.*, 1999, **101–103**, 847–850.
43 T. Mukherjee and P. Mukherjee, *Phys. Scr.*, 1999, **59**, 219–221.
44 M. Kavčič and K. Tökési, *Radiat. Phys. Chem.*, 2007, **76**, 542–545.
45 A. N. Nigam and S. N. Soni, *J. Phys. C: Solid State Phys.*, 1980, **13**, 1567–1570.
46 L. Parratt, *Phys. Rev.*, 1936, **49**, 502–507.
47 G. Graeffe, H. Juslén and M. Karras, *J. Phys. B: At. Mol. Phys.*, 1977, **10**, 3219–3227.
48 K. Yokoi, H. Oohashi, Y. Ito, T. Tochio and T. Shoji, *Radiat. Phys. Chem.*, 2006, **75**, 1461–1464.
49 S. S. Raju, B. S. Reddy, M. V. R. Murti and L. Mombasawala, *X-Ray Spectrom.*, 2007, **36**, 35–41.
50 C. H. Shaw and L. G. Parratt, *Phys. Rev.*, 1936, **50**, 1006–1012.
51 D. F. Anagnostopoulos, G. Borchert, D. Gotta, K. Rashid, D. H. Jakubassa-Amundsen and P. A. Amundsen, *Phys. Rev. A*, 1998, **58**, 2797–2814.
52 O. Mauron, J. C. Dousse, J. Hoszowska, J. P. Marques, F. Parente and M. Polasik, *Phys. Rev. A*, 2000, **62**, 062508.
53 H. Verma, *J. Phys. B: At., Mol. Opt. Phys.*, 2000, **33**, 3407–3415.
54 A. Li-Scholz, A. Leiberich and W. Scholz, *Phys. Rev. A*, 1982, **26**, 3232–3239.
55 S. Limandri, R. Bonetto, A. Carreras and J. Trincavelli, *Phys. Rev. A*, 2010, **82**, 032505.
56 I. Török and T. Bondár, *Nucl. Instrum. Methods Phys. Res., Sect. B*, 1999, **154**, 272–275.
57 S. J. Cipolla, *Nucl. Instrum. Methods Phys. Res., Sect. A*, 1999, **422**, 546.
58 C. Herren and J. Dousse, *Phys. Rev. A*, 1997, **56**, 2750.
59 S. N. Soni, *J. Phys. Chem. Solids*, 1996, **57**, 1831–1837.
60 M. Kavčič, J.-Cl. Dousse, J. Szlachetko and W. Cao, *Nucl. Instrum. Methods Phys. Res., Sect. B*, 2007, **260**, 642–646.
61 R. Alonso-Mori, E. Paris, G. Giuli, S. G. Eeckhout, M. Kavčič, M. Žitnik, K. Bučar, L. G. M. Pettersson and P. Glatzel, *Inorg. Chem.*, 2010, **49**, 6468–6473.
62 R. Alonso-Mori, E. Paris, G. Giuli, S. G. Eeckhout, M. Kavčič, M. Žitnik, K. Bučar, L. G. M. Pettersson and P. Glatzel, *Anal. Chem.*, 2009, **81**, 6516–6525.
63 S. Limandri, J. Trincavelli, R. Bonetto and A. Carreras, *Phys. Rev. A*, 2008, **78**, 022518.
64 G. Rémond, R. Myklebust, M. Fialin, C. Nockolds, M. Phillips and C. R. Carmes, *J. Res. Natl. Inst. Stand. Technol.*, 2002, **107**, 509–529.
65 R. Jenkins and J. DeVries, *Practical X-ray Spectrometry*, Springer-Verlag, New York, 2nd edn, 1982, p. 38.
66 R. Packwood and J. Brown, *X-Ray Spectrom.*, 1981, **10**, 138–145.
67 J. Riveros, G. Castellano and J. Trincavelli, *Mikrochim. Acta, Suppl.*, 1992, **12**, 99–105.
68 J. Trincavelli, S. Limandri, A. Carreras and R. Bonetto, *Microsc. Microanal.*, 2008, **14**, 306–314.
69 T. Tada, H. Fukuda, J. Hasegawa and Y. Oguri, *Spectrochim. Acta, Part B*, 2010, **65**, 46–50.
70 P. Pérez, A. Carreras and J. Trincavelli, *J. Phys. B: At., Mol. Opt. Phys.*, 2012, **45**, 025004.
71 T. Åberg, *Phys. Rev. A*, 1971, **4**, 1735–1740.
72 K. Tsutsumi, H. Nakamori and K. Ichikawa, *Phys. Rev. B*, 1976, **13**, 929–933.
73 H. Enkisch, C. Sternemann, M. Paulus, M. Volmer and W. Schülke, *Phys. Rev. A*, 2004, **70**, 022508.
74 H. Sörum, *J. Phys. F: Met. Phys.*, 1987, **17**, 417.
75 M. Oura, T. Mukoyama, M. Taguchi, T. Takeuchi, T. Haruna and S. Shin, *Phys. Rev. Lett.*, 2003, **90**, 173002.
76 E. Perino, M. Torres Deluigi, R. Olsina and J. A. Riveros, *X-Ray Spectrom.*, 2002, **31**, 115–119.